Waste Management 85 (2019) 333–340

Contents lists available at ScienceDirect

Waste Management

journal homepage: www.elsevier.com/locate/wasman

From polystyrene waste to porous carbon flake and potential application in supercapacitor

Jiakang Min [a,e], Shuai Zhang [b], Jiaxin Li [a], Rüdiger Klingeler [c], Xin Wen [a,b], Xuecheng Chen [a,b,*], Xi Zhao [d,*], Tao Tang [a,*], Ewa Mijowska [b]

[a] State Key Laboratory of Polymer Physics and Chemistry, Changchun Institute of Applied Chemistry, Chinese Academy of Sciences, Renmin Street 5625, Changchun 130022, China
[b] Nanomaterials Physicochemistry Department, Faculty of Chemical Technology and Engineering, West Pomeranian University of Technology, Szczecin, Piastów Ave. 42, 71-065 Szczecin, Poland
[c] Kirchhoff-Institut fürPhysik, Universität Heidelberg, INF 227, D-69120 Heidelberg, Germany
[d] Institute of Theoretical Chemistry, Jilin university, liutiao road 2#, Changchun, 130021, China
[e] University of Chinese Academy of Sciences, Beijing 100039, China

ARTICLE INFO

Article history:
Received 14 July 2018
Revised 21 December 2018
Accepted 1 January 2019

Keywords:
Waste recycling
Energy storage
Polystyrene waste
Porous carbon flake
Manganese dioxide
Supercapacitor

ABSTRACT

Due to white pollution related environmental concern and sustainable development requirement, it is desirable to recycle the widely used plastic wastes into products with commercial value, such as high-valued carbon materials which can be applied in electrochemical fields. In this work, porous carbon flakes (PCFs) are produced by direct pyrolysis of polystyrene waste through template method. Furthermore, manganese dioxide (MnO_2) nanosheets are selectively deposited on the surface of resultant PCFs to form hybrid (PCF-MnO_2). Because of the large specific surface area (1087 m^2/g) and high conductivity of PCFs, native high specific capacity of MnO_2, and positive synergistic interaction between PCF and MnO_2, the resulting hybrid materials show an ultrahigh capacitance of 308 F/g at 1 mV/s and 247 F/g at 1 A/g in LiCl electrolyte, and excellent cycle stability of 93.4% capacitance retention over 10,000 cycles at 10 A/g in symmetric supercapacitor device. This work demonstrates a convenient method for the preparation of cost-effective and high-performance electrode material for electric capacitor. More importantly, it provides a potential way to recycle polystyrene waste into high-valued product in large-scale with disposing of polymeric waste to alleviate environmental concerns.

1. Introduction

Nowadays, along with the development of petroleum industry, synthetic polymers such as polypropylene (PP), polyethylene (PE) and polystyrene (PS) are becoming indispensable parts of our lives, but meanwhile as the most problematic sources of wastes for mankind. For example, there are about 3 million tons of PS waste produced and discarded annually which are causing serious white environmental pollution because of their chemical stability (Hearon et al., 2014). Currently landfill and incineration are the two common ways to dispose of plastic wastes (Pol, 2010). However, landfill has to face continuous cost increases, long-term environmental concerns and diminishing space while incineration has disadvantages of high energy consumption and toxic gas release. Therefore, it is imperative to make alternative treatment options for sustainable and eco-friendly recycling of polymeric wastes (Baytekin et al., 2013).

Considering the abundance of carbon element in polymers, carbonization of polymeric wastes to carbon material is one of the most promising recycling strategies (Pol, 2010). Furthermore, the morphology and structure of resultant carbon products can be selectively controlled to meet the demand for various applications (Hong et al., 2012). So far, many kinds of polymers, such as PP and PE have been successfully carbonized into carbon nanotubes (CNT), carbon hollow spheres (HCS), porous carbon sheets (PCS) and so on (Gong et al., 2014). However, PS is chemically inert and hard to degrade without any special treatments (Jang and Wilkie, 2005). As far, there are only several reports on the synthesis of carbon materials from PS, such as introduction of negatively-charged sulfonate groups (Lv et al., 2015) or combined catalysts ($AlCl_3$ and CCl_4) (Li et al., 2006) to crosslink the PS matrix. Despite these progresses have been made, it is still a great challenge to develop simple and efficient methods to produce porous carbon materials from

* Corresponding authors at: Nanomaterials Physicochemistry Department, Faculty of Chemical Technology and Engineering, West Pomeranian University of Technology, Szczecin, Piastów Ave. 42, 71-065 Szczecin, Poland (X. Chen).
E-mail addresses: xchen@ciac.ac.cn (X. Chen), zhaoxi@jlu.edu.cn (X. Zhao), ttang@ciac.ac.cn (T. Tang).

https://doi.org/10.1016/j.wasman.2019.01.002
0956-053X/

PS with controllable morphology. According to recent reports of our group, we found that the template method is a special and effective solution to achieve above goal (Gong et al., 2013; Ma et al., 2018; Wen et al., 2015). Using template method, the parameters, such as morphology, porosity properties and conductivity of template derived materials can be well controlled to meet defined applications (Shen et al., 2018). In this respect, polymer derived carbon materials featuring special parameters is highly depending on the template used (Zhao et al., 2017). Up to now, MgO has been demonstrated as the most favorable catalysts and templates for the synthesis of high-quality porous graphene materials (Zhao et al., 2015). Moreover, MgO is attractive because of its low cost, facile purification, tunable morphologies and pore size and as well as can be easily removed by a non-corrosive acid, which make it widely used in polymer nanocomposites. Base on above premises, it is imperative to develop a reliable method to prepare carbon nanomaterials from MgO templates.

Supercapacitors have attracted considerable attention because of their long cycle life, fast charge/discharge rate, and high power density (Dutta et al., 2017; Min et al., 2017; Shieh et al., 2013; Shieh et al., 2015; Song et al., 2018; Sun et al., 2012; Xue et al., 2018). According to the energy storage mechanism, there are two kinds of supercapacitors, electronic double layer capacitor (EDLC) and pseudocapacitor. The electrode materials of pseudocapacitor are generally transition metal oxide, such as RuO_2, MnO_2, NiO and so on. The manganese dioxide (MnO_2) is a most promising pseudocapacitive material due to its high theoretical specific capacity (1370 F/g), cost effectiveness and environmental benignity. However, inherent the poor conductivity limits the charge-discharge rate for high-power application (Simon and Gogotsi, 2008). To address this problem, varies of strategies have been developed, for example, MnO_2 has been combined with graphene, CNT and HCS to improve the electric conductivity (Li et al., 2015; Liu et al., 2016; Liu et al., 2017; Peng et al., 2013; Wang et al., 2017; Zhao et al., 2014). Although many achievements have been made, the synthesis methods reported in the literature tend to be relatively complicated and time consuming and are not suitable for sustainable large-scale production, it is still imperative to exploit an effective method to prepare carbon materials-MnO_2 composite to further improve the supercapacitive performance.

In this work, a hybrid (PCF-MnO_2) electrode material from carbonization of PS foam waste is developed by a template to achieve the above goal. First of all, porous carbon flakes (PCFs) are prepared by direct pyrolysis of PS foam waste in a stainless steel autoclave using flake structured MgO as the template. Subsequently, MnO_2 nanosheets are selectively deposited on the surface of resultant PCFs to form hybrid (PCF-MnO_2). Owing to the large specific surface area (1087 m^2/g) and high conductivity of PCFs, native high specific capacity of MnO_2, positive synergistic interaction between PCF and MnO_2, the resulting hybrid materials show an ultrahigh capacitance of 308 F/g at 1 mV/s and 247 F/g at 1 A/g in LiCl electrolyte, and excellent long term stability of 93.4% capacitance retention over 10,000 cycles at 10 A/g in symmetric supercapacitor device. This work demonstrates a convenient method for the preparation of cost-effective and high-performance electrode material for electric capacitor. More importantly, it provides a potential way to recycle polystyrene waste into high-valued product in large-scale with disposing of polymeric waste to alleviate environmental concerns.

2. Experimental section

2.1. Materials

PS was obtained from the commercial polystyrene foam package. Porous flake structured MgO, hydrochloric acid (HCl, 5%), and ethanol (98%) were purchased from China National Medicines Corporation Ltd. And potassium permanganate ($KMnO_4$) was brought from Sigma-Aldrich. All the chemicals are directly used without further purification.

2.2. Synthesis of PCF

In a typical synthesis, 2 g of porous flake structured MgO and 0.2 g of PS were mixed and introduced to an autoclave at room temperature. The autoclave was sealed and heated at a rate of 20 K/min and then held at 973 K for 2 h. After cooling down to room temperature, black solid samples were collected and then mixed with diluted HCl to remove the MgO template. The mixtures were filtered and rinsed several times with deionized water and the PCF was then dried at 353 K for 8 h in a vacuum.

2.3. Preparation of PCF-MnO_2 hybrid

In a typical synthesis, the obtained PCFs (10 mg) and $KMnO_4$ (5 mg) were dispersed in 50 ml of ethanol and sonicated for 1 h at room temperature. After filtration and rinsed several times with deionized water and ethanol, the solid product PCF-MnO_2 was then dried at 353 K for 8 h in a vacuum oven.

2.4. Characterization

The morphology and microstructure of the samples were examined by field-emission scanning electron microscopy (FE-SEM, JEOLJEM-1011) at 100 kV and transmission electron microscopy (TEM, FEI G2 S-T) and high-resolution transmission electron microscope (HRTEM) on a FEI G2 S-Twintransmission electron microscope operating at 200 kV. The relative molecular weight of PS foam was determined by gel permeation chromatography (GPC) on TOSOH HLC 8220 GPC at 40 °C using THF as an eluent against linear polystyrene standards. The height images of the PCFs was acquired using tapping-mode atomic force microscopy (AFM) with a hot stage (Nanoscope IIIa MultiMode, Digital Instruments). The sample for AFM observation was prepared by spin-coating on a clean silicon wafer at room temperature. The phases were determined by X-ray diffraction (XRD, D8 advance X-ray diffractometer) with Cu K_α radiation at 40 kV and 200 mA. The thermal stability of the samples was measured by thermal gravimetric analysis (TGA) under flowing air at a heating rate of 10 K/min on the TA Instrument SDT Q600. The vibrational properties were characterized by Raman scattering (T6400, excitation-beam wavelength: 514.5 nm) and the porosities were measured by nitrogen adsorption/desorption at 77 K on a Quantachrome Autosorb-1C-MS analyzer.

2.5. Electrochemical measurements

The three-electrode capacitor was composed of PCFs. To fabricate electrodes, PCFs (80 wt%) were mixed with Super-P (10 wt%) and polytetrafluoroethylene (binder, (10 wt%)) in ethanol to form homogeneous slurry. The slurry was coated onto a porous 3D-nickel foam (1.2 mm thick, as current collector) with mass loading of 4 mg/cm^2, which was highly compressible. The preform (electrode) structure was dried under vacuum at 100 °C for 10 h to remove ethanol, before being compressed into a disk to form the electrode. The final electrode was $\sim$10$\times$ thinner than the original foam thickness which was around 0.12 mm. In three-electrode cells, in addition to the working electrode of active material, 6 M KOH as the electrolyte and Ag/AgCl as the reference electrodes were used. Cyclic voltammetry (CV) test and galvanostatic charge-discharge (GCD) test were performed using an electrochemical analyzer, CHI 660E, under ambient conditions. Electric

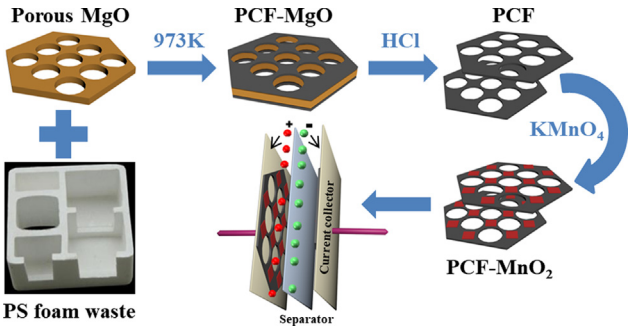

Scheme 1. Schematic illustration for the formation of PCF and PCF-MnO_2 hybrid.

impedance spectroscopy was performed with an amplitude of 10 mV, from 10 mHz to 10 kHz. The two-electrode capacitor was composed of PCFs and PCF-MnO_2, respectively. The electrodes with a diameter of 10 mm were pressed from a mixture of the active materials (85%), polyvinylidene fluoride (10%) and multi-wall carbon nanotubes (5%, 20–40 nm in diameter) with mass loading of 2 mg/cm^2. The electrodes were separated by glassy fibrous paper and placed between iron current collectors in a teflon Swagelok® type system in which 6 M KOH and 5 M LiCl were the electrolyte. The electrochemical performances were evaluated by cyclic voltammetry (CV), galvanostatic charge/discharge (GCD) and electrochemical impedance spectroscopy (EIS) measurements using two-electrode system with an EC-LAB VMP3 (BioLogic Science Instruments). The CV curves were performed under a potential

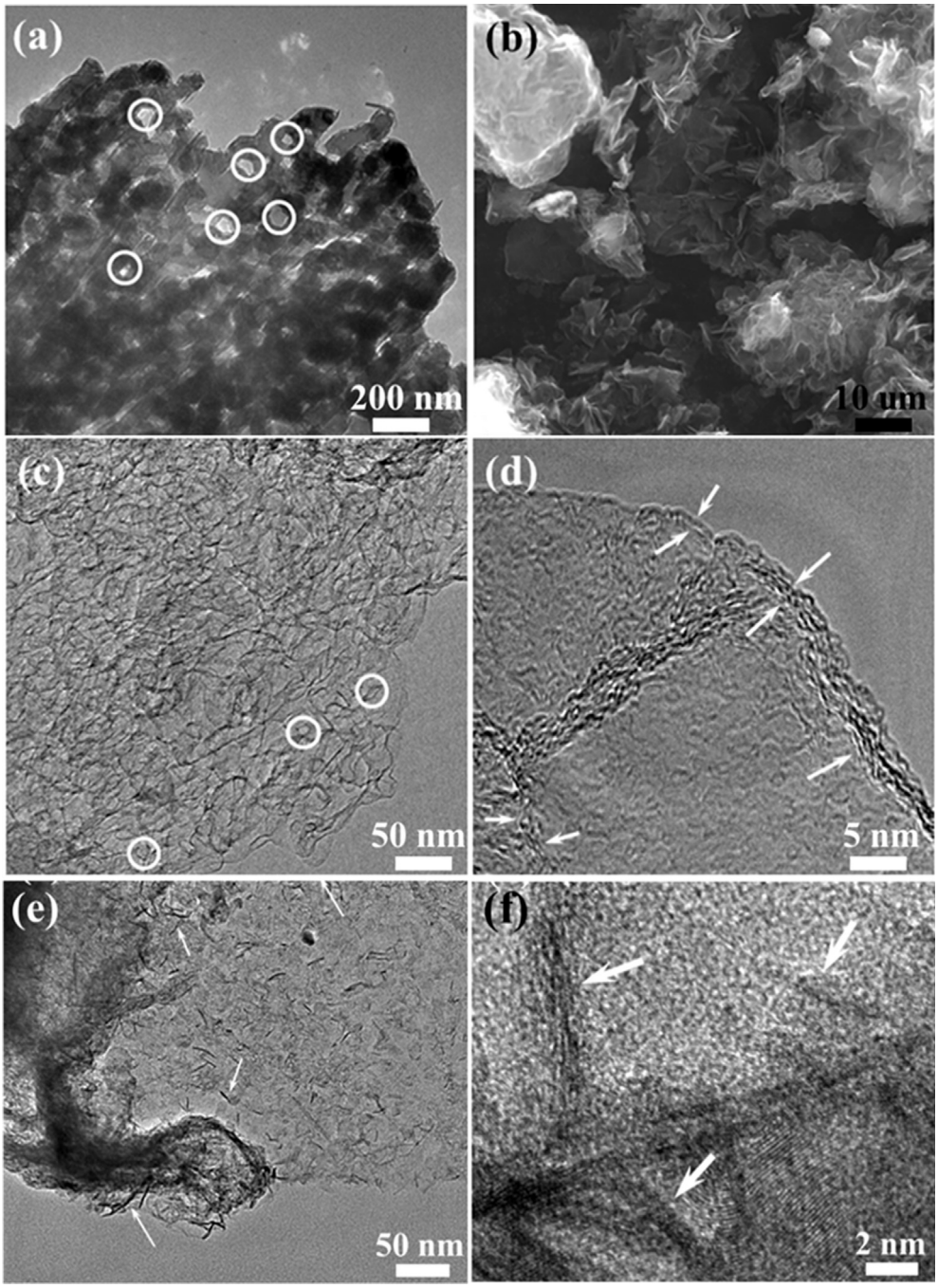

Fig. 1. TEM images of (a) MgO template and (b) SEM image of prepared PCF from MgO, (c, d) TEM images of PCF and (e, f) TEM images of PCF-MnO_2 hybrid.

window from 0–0.7 V at different scan rates in the range from 1 to 200 mV s^{-1}. GCD measurements were investigated in potential window from 0 to 0.7 V at different current densities from 1 to 20 A/g. EIS was taken in the frequency range from 100 kHz to 1 mHz with an amplitude of 10 mV.

The capacitance calculated from CV curve was from the following equation:

$$C = \frac{1}{m \times \Delta v \times s}\left(\int_{v_0}^{v} id v + \int_{v}^{v_0} id v\right)$$

where C is the capacitance (F/g), m is the mass loading of active material, Δv is the voltage window in the measurement, s is the scan speed for each CV measurement. Integral is the area of each CV curve.

In two electrode system, capacitance calculated from GCD curve was from the following equation:

$$C = \frac{2 \times I \times \Delta t}{m \times \Delta U}$$

where the C is capacitance (F/g), Δt is the discharge time of GCD measurement, m is the mass loading of active material in one tablet, ΔU is the voltage window in the measurement.

3. Results and discussion

As presented in Scheme 1, during the carbonization process of PS foam waste, the carbonization environment is inert atmosphere and requires an autoclave and high temperatures. According to the generally accepted dissociation–diffusion–precipitation mechanism for the growth of carbon (Amelinckx et al., 1994), the PS waste is firstly decomposed into small organic molecules (light hydrocarbons gas mainly consisted of hydrogen, methane, ethane, ethylene, propane, propylene, i-butene, and pentene and aromatics) (Ma et al., 2018; Wen et al., 2015) which evaporated inside the autoclave. Subsequently, these organic molecules are dehydrogenated and aromatized on the MgO template surface to form a thin carbon layer. After removing the MgO template, PCFs are obtained with yield around 25%. Finally, PCF-MnO_2 hybrid is prepared by spontaneous redox deposition of MnO_2 on PCF. According to the literature (Bao et al., 2011; Fischer et al., 2007; Lee et al., 2010; Ma et al., 2007), the spontaneous redox deposition of MnO_2 on carbon materials is pH-dependent. In neutral $KMnO_4$ solutions, thin films of MnO_2 can be obtained on the surface of carbon. The as-prepared PCF-MnO_2 is directly used as electrode materials for the construction of two electrode supercapacitor.

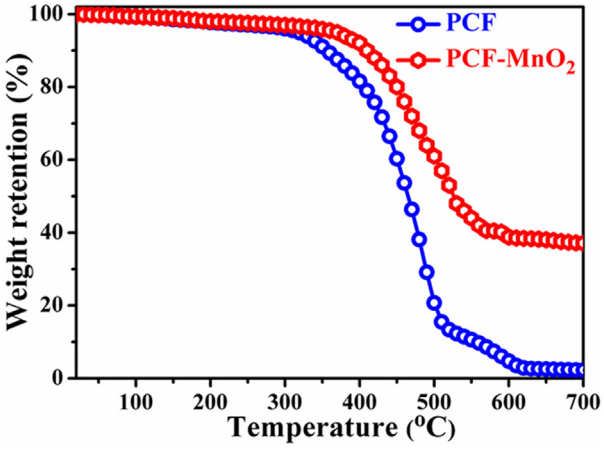

Fig. 2. TGA curves of PCF and PCF-MnO_2 hybrid.

The number-average molecular weights (M_n = 57000 g/mol) and polydispersity indices (PDI = 2.64) of the PS foam waste are examined by GPC measurement (Fig. S1). In order to characterize that the structure of PCFs prepared from MgO template, the morphology of PCFs is examined by SEM and TEM, respectively. Fig. 1a is the TEM image of the MgO template, in which the open pores are clearly observed and sizes are in the range of 10–100 nm as indicated by white circles. Fig. 1b is the SEM image of prepared PCFs from MgO template. It is found that thin layers of PCFs are formed and aggregated together. Fig. 1c depicts the TEM image of PCFs revealing a porous flake structure. Many thin layers of carbon with small pores could be observed and the sizes of pores are consistent with the pores from MgO template, suggesting that the morphology of PCF inherited from the MgO template which meant the pores of PCFs are derived from porous MgO. In order to characterize the morphology of PCFs in detail, it finds that the carbon flakes are composed of several layers of graphitic carbon as indicated by with white arrows in Fig. 1d and AFM images in Fig. S2. As shown in Fig. 1e and f with white arrows, MnO_2 nanosheets are successfully supported onto the surfaces of PCFs. The as-prepared MnO_2 evenly distributed on the PCFs are confirmed by energy-dispersive spectroscopy (EDS) elemental mapping (Fig. S3). In XPS spectroscopy (Fig. S4), the Mn 2p spectrum of PCF-MnO_2 exhibits two characteristic peaks at 642.0 eV and 653.8 eV, respectively, corresponding to the Mn $2p^{3/2}$ and Mn $2p^{1/2}$ peaks of MnO_2. From above analysis, it is confirmed that MnO_2 has been successfully supported on PCFs.

The corresponding TGA profiles of PCFs and PCF-MnO_2 are shown in Fig. 2. The ash content of PCFs is close to 0% demonstrat-

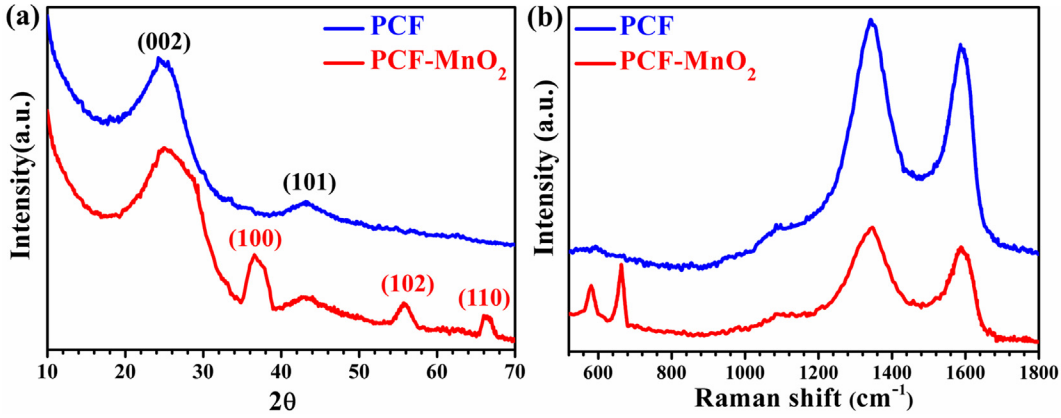

Fig. 3. (a) XRD pattern and (b) Raman scattering spectra of PCF and PCF-MnO_2 hybrid.

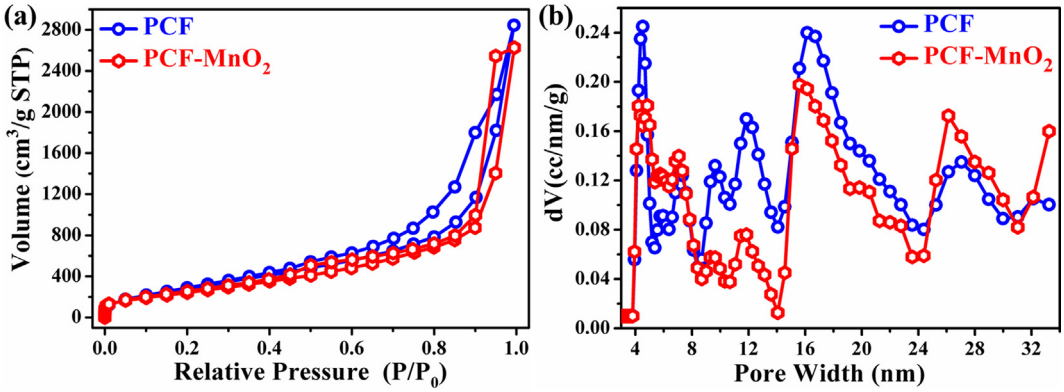

Fig. 4. (a) N_2 sorption/desorption isotherm, (b) pore size distribution of PCF and PCF-MnO_2 hybrid.

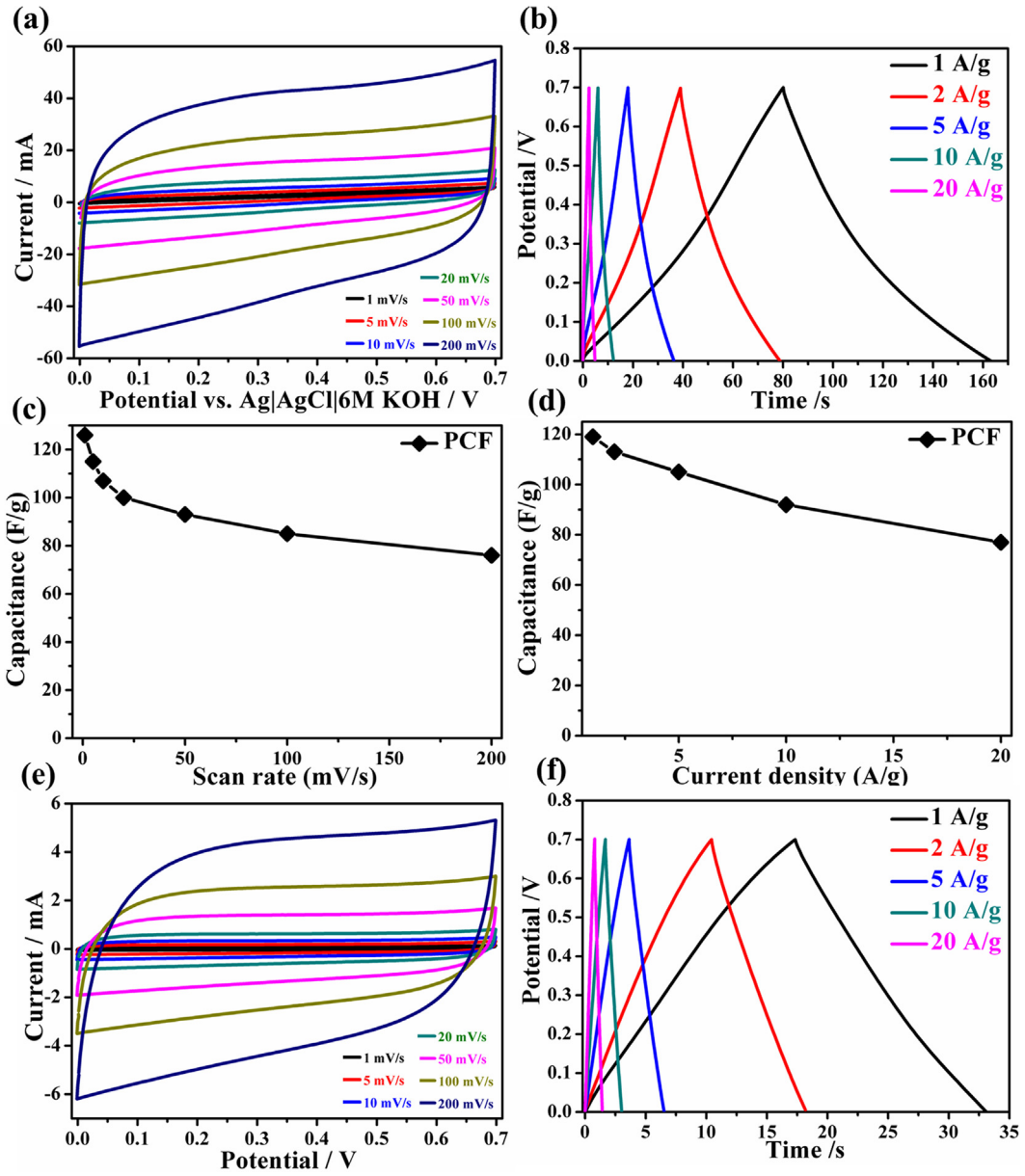

Fig. 5. Three electrode system results for (a) CV and (b) GCD curves of PCF, (c) specific capacitance at different scan rates and (d) at different current densities two electrode system results for (e) CV and (f) GCD curves of PCF performed in KOH electrolyte.

ing that MgO template has been completely removed from the carbon materials and there is about 37% of MnO_2 supported on the resultant PCFs. The powder XRD patterns of the PCFs and PCF-MnO_2 are shown in Fig. 3a. There are two strong and broad peaks at 26° and 43° at the same reciprocal spacing as the (0 0 2) and (1 0 1) carbon reflections respectively, showing that the PCFs are composed of disordered graphitic carbon. The peaks of PCF-MnO_2 at $2\theta = 36.6°$, 55.2° and 65.7° are associated with the (1 0 0), (1 0 2), and (1 1 0) planes of the ε-MnO_2 (JCPDS 00-030-0820), which suggests that MnO_2 has been successfully supported on PCFs. The bonding, order, and crystallinity of the PCFs and PCF-MnO_2 are further characterized by Raman spectroscopy. As shown in Fig. 3b, there are two Raman modes in PCFs and PCF-MnO_2 samples, D and G bands at around 1330 and 1600 cm^{-1}. The peak at 1600 cm^{-1} (G band) is related to sp^2-hybridized carbon atoms in a graphite layer. The D band at 1330 cm^{-1} is associated with carbon atoms with dangling bonds in the plane termination of disordered graphite. The intensity ratio of the G and D bands (I_G/I_D) of PCFs is 0.79, it indicates that the PCFs prepared from MgO template are composed of ordered and disordered graphitic carbons. In PCF-MnO_2 sample, another two strong peaks at 575 and 648 cm^{-1} are observed, which are ascribed to MnO_2. This further proves that the results of Raman spectra agree well with XRD and TEM. The porosity of PCFs and PCF-MnO_2 are investigated by N_2 adsorption/desorption experiments (Fig. 4a). According to the IUPAC classification on porosity, PCFs and PCF-MnO_2 both are type-IV isotherm with a high nitrogen adsorption capacity at middle relative pressure, indicative of their mesoporous structure existed in PCFs and PCF-MnO_2 sample (Liu et al., 2015; Ma et al., 2014), as confirmed by the corresponding pore size distribution curves (Fig. 4b). According to QSDFT method, the pores size of PCFs are centered at 4.3, 7.8, 9.6, 12.2, 17.3, 27.4 and 32.1 nm, while PCF-MnO_2 are centered at 4.5, 7.7, 9.4, 11.8, 16.5, 26.7 and 33.8 nm, as shown in Fig. S5. The Brunauer-Emmett-Teller (BET) specific surface area and pore volume are 1087 m^2/g and 4.42 cm^3/g for PCF, 911 m^2/g and 4.19 cm^3/g for PCF-MnO_2, respectively. As shown in Fig. 1f, it is found the MnO_2 nanosheets are porous. The specific surface area of PCF has only decreased 16.2% after coating the MnO_2. From N_2 sorption/desorption analysis, it is confirmed that PCFs and corresponding PCF-MnO_2 hybrid materials are highly porous, which is favorable for supercapacitor applications.

Since the as-synthesized PCFs exhibit large specific surface area, pore volume and hierarchical porosity properties, it is further evaluated as the electrode material for supercapacitor. As shown in Fig. 5a, in three electrode cells, the cyclic voltammetry (CV) curves show a nearly rectangular shape at high sweep rates, indicative good EDLC capacitor behaviors of PCFs. Fig. 5b shows galvanostatic charging/discharging (GCD) curves with isosceles triangle shape, implying a small equivalent series resistance and excellent capacitive nature of PCFs. The specific capacitances at different scan rates and current densities are presented in Fig. 5c and d. The specific capacitances are 126 F/g at a scan rate of 1 mV/s and 119 F/g a current density of 1 A/g, respectively. The supercapacitive performance of PCFs is further performed in the symmetric system. In two electrode cells, it delivers a specific capacitance of 61 F/g at 1 mV/s and 50 F/g at 1 A/g in KOH electrolyte (Fig. 5e and f), and 33 F/g at 1 mV/s and 26 F/g at 1 A/g in LiCl electrolyte, respectively (Fig. S6a and b). According to Chmiola's work, as the carbon electrode materials for supercapacitor, only the pore size matches well with the size of electrolyte ions can achieve high specific capacitance (Chmiola et al., 2006). The low capacitance of PCFs in the symmetric system could be ascribed to the large pore sizes of PCFs which resulted in a decrease in their specific surface area.

In order to further improve the specific capacitance of PCFs, MnO_2 is subsequently loaded on PCF to get the PCF-MnO_2 hybrid material, and tested in 5 M LiCl neutral electrolyte in two electrode

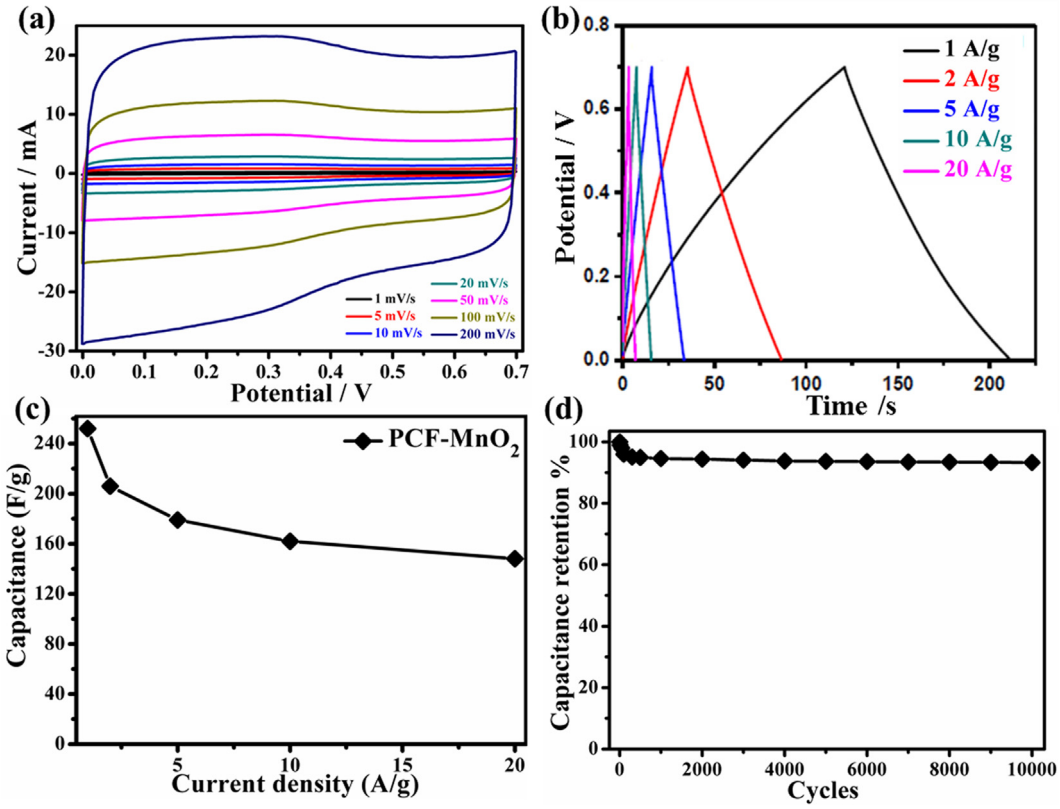

Fig. 6. (a) CV and (b) GCD curves of PCF-MnO_2 (c) Specific capacities of PCF-MnO_2 at different current densities and (d) Cycling stability of PCF-MnO_2 at 10 A/g.

Table 1
Comparison of specific capacitances with other MnO_2-based symmetric dual supercapacitor.

Materials[a]	Capacity (F/g)	Capacity (F/g)	Stability	Ref./Year
MnO_2/GNS	267 (0.2 A/g)		92% (7000)	Peng/2013
C@MnO_2 (45%)		252 (2 mV/s)	74% (2000)	Zhao/2014
MnO_2@CCNs (75%)	189 (1 A/g)		95% (10000)	Li/2015
NGMn		250 (5 mV/s)	90% (1500)	Liu/2016
RGO/MnO_x@HCN (20%)	270 (1 A/g)		88% (5000)	Liu/2017
r-GO/MnO_x		202 (1 mV/s)	106% (115000)	Wang/2017
PCF-MnO_2 (37%)	247 (1 A/g)	308 (1 mV/s)	93% (10000)	Our work

[a] The percentage respresents the loadigng amounts of MnO_2.

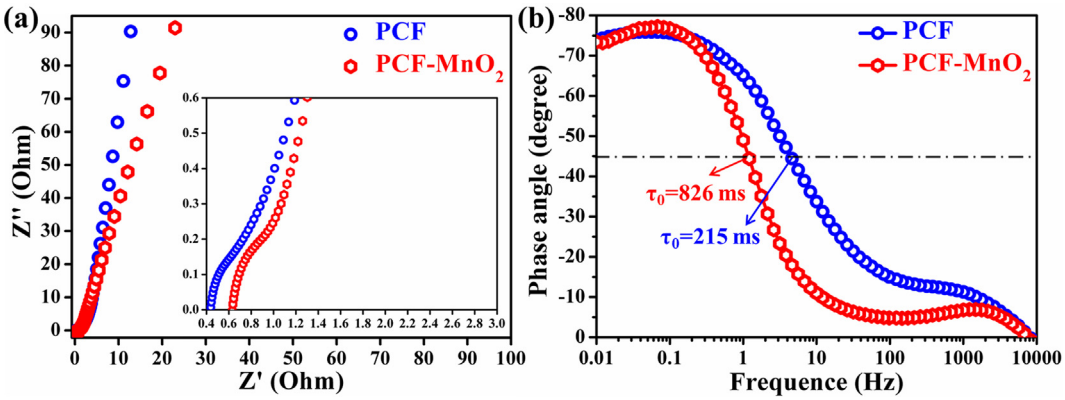

Fig. 7. (a, b) Nyquist plots and the respective Bode plots and inset in (a) magnifies the high-frequency range of PCF and PCF-MnO_2.

configurations. The type for supercapacitor was a symmetrical supercapacitor with both positive electrode and negative electrode of PCF-MnO_2 hybrid material. Fig. 6a shows the CV curves of PCF-MnO_2, which delivers the specific capacitance of 308 F/g at a scan rate of 1 mV/s. In Fig. 6b and c, it shows the GCD curves of PCF-MnO_2 at different current densities. At a current density of 1 A/g, the specific capacity is 247 F/g. Further increase the current density to 20 A/g, a high capacitance of 141 F/g still can be obtained. In sharp contrast, under the same conditions, the neat MnO_2 shows negligible capacitance and PCFs also show very low specific capacitance of 26 F/g (Fig. S6). Based on the above analysis, it is confirmed that there is positive synergistic effect between PCFs and MnO_2 nanosheets, which dramatically improves the conductivity of PCF-MnO_2 hybrid materials leading to the high specific capacitance achieved. The long cycle stability is crucial parameter to evaluate the electrochemical performance of supercapacitors. As shown in Fig. 6d, after 10,000 cycles, PCF-MnO_2 still remains about the 93.4% of the initial capacitance at a high current density of 10 A/g, exhibiting an excellent cycling stability. Moreover, Table 1 summarizes the comparisons with previously reported MnO_2-based supercapacitor, revealing that PS-derived PCF-MnO_2 has the even better results than those of recently reported MnO_2 based supercapacitor.

For understanding the origin of the advanced supercapacitive performance, we use classical electrochemical impedance spectroscopy to investigate the structure-performance relationship of the supercapacitors as shown in Fig. 7. The nearly vertical Nyquist plots in the low-frequency region demonstrate the ideal capacitive behavior of PCFs and PCF-MnO_2. The enlarged high-frequency region presents a transition from the vertical curve to the 45° Warburg region followed by a semicircle (inset in Fig. 7a). By extrapolating the vertical portion to the real axis, the remarkably small R_{ESR} of 0.41 and 0.63 Ω are obtained for PCFs and PCF-MnO_2, respectively, which are consistent with the very limited *IR* drops in GCD curves. Such small R_{ESR} values are related to high conductivity and the hierarchical porous structure, which provides a rapid ion diffusion channel and a short diffusion distance by the interconnected micro-meso-macropores. In the Bode plots, the characteristic frequency f_0 at the phase angle of −45°for PCF and PCF-MnO_2 are 4.65 and 1.21 Hz, corresponding to the time constant τ_0 ($\tau_0 = 1/f_0$) of 215 and 826 ms, respectively (Fig. 7b). The τ_0 values are greatly smaller than those of the conventional activated-carbon supercapacitors (10 s), indicating the faster charge/discharge rate of PCF-based supercapacitors.

4. Conclusions

Highly porous carbon flakes are prepared from PS waste using flake structured MgO as the template. The obtained PCFs are used directly as the carbon support for the deposition of MnO_2 nanosheets. As the electrode materials in a two electrode supercapacitor, the PCF-MnO_2 hybrid materials exhibit excellent electrochemical properties including a high capacity of 247 F/g at a current density of 1 A/g, 308 F/g at a scanning rate of 1 mV/s and long term stability of 93.4% after 10,000 cycles at 10 A/g. The present work provides a practical way to recycle polymeric waste and convert it into products with high value while alleviating environmental concerns.

Notes

Declarations of interest: none.

Author contributions

All authors have given approval to the final version of the manuscript.

Acknowledgment

This work was supported by the National Natural Science Foundation of China (Project Nos. 51303170) and National Science Centre, Poland within SONATA BIS 2015/18/E/ST8/00291.

Appendix A. Supplementary material

GPC image of the PS foam, EDS and XPS pattern of PCF-MnO_2, CV curves and specific capacities of MnO_2 at different scan rates are provided in the Supporting Information. Supplementary data to this article can be found online at https://doi.org/10.1016/j.wasman.2019.01.002.

References

Amelinckx, S., Zhang, X.B., Bernaerts, D., Zhang, X.F., Ivanov, V., Nagy, J.B., 1994. A formation mechanism for catalytically grown helix-shaped graphite nanotubes. Science 265, 635–639.

Bao, L., Zang, J.F., Li, X.D., 2011. Flexible Zn_2SnO_4/MnO_2 core/shell nanocable-carbon microfiber hybrid composites for high-performance supercapacitor electrodes. Nano Lett. 11, 1215–1220.

Baytekin, B., Baytekin, H.T., Grzybowski, B.A., 2013. Retrieving and converting energy from polymers: deployable technologies and emerging concepts. Energy Environ. Sci. 6, 3467–3482.

Chmiola, J., Yushin, G., Gogotsi, Y., Portet, C., Simon, P., Taberna, P.L., 2006. Anomalous increase in carbon capacitance at pore sizes less than 1 nanometer. Science 313, 1760–1763.

Dutta, S., Kim, J., Ide, Y., Kim, J., Yamauchi, Y., Wu, K.C.-W., 2017. 3D network of cellulose-based energy storage devices and related emerging applications. Mater. Horiz. 4, 522–545.

Fischer, A.E., Pettigrew, K.A., Rolison, D.R., Long, J.W., 2007. Incorporation of homogeneous, nanoscale MnO_2 within ultraporous carbon structures via self-limiting electroless deposition: implications for electrochemical capacitors. Nano Lett. 7, 281–286.

Gong, J., Liu, J., Chen, X.C., Wen, X., Jiang, Z.W., Mijowska, E., Wang, Y.H., Tang, T., 2013. Synthesis, characterization and growth mechanism of mesoporous hollow carbon nanospheres by catalytic carbonization of polystyrene. Micropor. Mesopor. Mat. 176, 31–40.

Gong, J., Liu, J., Chen, X.C., Wen, X., Mijiwska, E., Tang, T., 2014. Converting mixed plastics into mesoporous hollow carbon spheres with controllable diameter. Appl. Catal. B: Environ. 152, 289–299.

Hearon, K., Nash, L.D., Rodriguez, J.N., Lonnecker, A.T., Raymond, J.E., Wilson, T.S., Wooley, K.L., Maitland, D.J., 2014. A high-performance recycling solution for polystyrene achieved by the synthesis of renewable poly(thioether) networks derived from D-limonene. Adv. Mater. 26, 1552–1558.

Hong, N.N., Wang, B.B., Song, L., Hu, S., Tang, G., Wu, Y., Hu, Y., 2012. Low-cost, facile synthesis of carbon nanosheets by thermal pyrolysis of polystyrene composite. Mater. Lett. 66, 60–63.

Jang, B.N., Wilkie, C.A., 2005. The thermal degradation of polystyrene nanocomposite. Polymer 46, 2933–2942.

Lee, S.W., Kim, J., Chen, S., Hammond, P.T., Shao-Horn, Y., 2010. Carbon nanotube/manganese oxide ultrathin film electrodes for electrochemical capacitors. ACS Nano 4, 3889–3896.

Li, L.C., Song, H.H., Chen, X.H., 2006. Hollow carbon microspheres prepared from polystyrene microbeads. Carbon 44, 587–610.

Li, Y.J., Yu, N., Yan, P., Li, Y.G., Zhou, X.M., Chen, S.L., Wang, G.L., Wei, T., Fan, Z.J., 2015. Fabrication of manganese dioxide nanoplates anchoring on biomass derived cross-linked carbon nanosheets for high-performance asymmetric supercapacitors. J. Power Sources 300, 309–317.

Liu, Y.C., Miao, X.F., Fang, J.H., Zhang, X.X., Chen, S.J., Li, W., Feng, W.D., Chen, Y.Q., Wang, W., Zhang, Y.N., 2016. Layered-MnO_2 nanosheet grown on nitrogen-doped carbon template as a composite cathode for flexible solid-state asymmetric supercapacitor. ACS Appl. Mater. Interfaces 8, 5251–5260.

Liu, M.X., Qian, J.S., Zhao, Y.H., Gan, L.H., Chen, L.W., 2015. Core–shell ultramicroporous@microporous carbon nanospheres as advanced supercapacitor electrodes. J. Mater. Chem. A 3, 11517–11526.

Liu, M.X., Shi, M.C., Lu, W.J., Zhu, D.Z., Li, L.C., Gan, L.H., 2017. Core–shell reduced graphene oxide/MnO_x@carbon hollow nanospheres for high performance supercapacitor electrodes. Chem. Eng. J. 313, 518–526.

Lv, W.M., Xiang, J.Y., Wen, F.S., Jia, Z.Y., Yang, R.L., Xu, B., Yu, D.L., He, J.L., Liu, Z.Y., 2015. Chemical vapor synthesized WS_2-embedded polystyrene-derived porous carbon as superior long-term cycling life anode material for Li-ion batteries. Electrochim. Acta 153, 49–54.

Ma, J.L., Liu, J., Song, J.F., Tang, T., 2018. Pressurized carbonization of mixed plastics into porous carbon sheets on magnesium oxide. RSC Adv. 8, 2469–2476.

Ma, S.B., Ahn, K.Y., Lee, E.S., Kim, K.B., 2007. Synthesis and characterization of manganese dioxide spontaneously coated on carbon nanotubes. Carbon 45, 375–382.

Ma, X.M., Gan, L.H., Liu, M.X., Zhao, Y.H., Chen, L.W., 2014. Mesoporous size controllable carbon microspheres and their electrochemical performances for supercapacitor electrodes. J. Mater. Chem. A 2, 8407–8415.

Min, J.K., Kierzek, K., Chen, X.C., Chu, P.K., Zhao, X., Kaleoczuk, R.J., Tang, T., Mijowska, E., 2017. Facile synthesis of porous iron oxide/graphene hybird nanocomposites and potential application in electrochemicalf energy storage. New J. Chem. 41, 13553.

Peng, L., Peng, X., Liu, B., Wu, C.Z., Xie, Y., Yu, G.H., 2013. Ultrathin two-dimensional MnO_2/graphene hybrid nanostructures for high-performance, flexible planar supercapacitors. Nano Lett. 13, 2151–2157.

Pol, V.G., 2010. Upcycling: converting waste plastics into paramagnetic, conducting, solid, pure carbon microspheres. Environ. Sci. Technol. 44, 4753–4759.

Shen, K., Zhang, L., Chen, X.D., Liu, L.M., Zhang, D.L., Li, Y.W., Chen, B.L., 2018. Ordered macro-microporous metalorganic framework single crystals. Science 359, 206–210.

Shieh, F., Hsiao, C., Kao, H., Wu, C., Chen, X., Tsung, C.-K., Wu, K.C.-W., 2013. RSC Adv. 3, 25686–25689.

Shieh, F., Wang, S., Yen, C., Wu, C., Dutta, S., Wu, K.C.-W., Tsung, C.-K., 2015. Imparting functionality to biocatalysts via embedding enzymes into nanoporous materials by a de novo approach: size-selective sheltering of catalase in metal-organic framework microcrystals. J. Am. Chem. Soc. 137, 4276–4279.

Simon, P., Gogotsi, Y., 2008. Materials for electrochemical capacitors. Nat. Mater. 7, 845–854.

Song, Z., Zhu, D., Xue, D., Liu, M.X., Gan, L.H., 2018. Nitrogen-enriched hollow porous carbon nanospheres with tailored morphology and microstructure for all-solid-state symmetric supercapacitors. ACS Appl. Energy Mater. 1, 4293–4303.

Sun, G.H., Wang, J., Li, K.X., Li, Y.Q., Xie, L.J., 2012. Polystyrene-based carbon spheres as electrode for electrochemical capacitors. Electrochim. Acta 59, 424–428.

Wang, Y., Lai, W.H., Wang, N., Jiang, Z., Wang, X.Y., Zou, P.C., Lin, Z.Y., Fan, H.J., Kang, F.Y., Wong, C.P., Yang, C., 2017. A reduced graphene oxide/mixed-valence manganese oxide composite electrode for tailorable and surface mountable supercapacitors with high capacitance and super-long life. Energy Environ. Sci. 10, 941–949.

Wen, Y.L., Liu, J., Song, J.F., Gong, J., Chen, H., Tang, T., 2015. Conversion of polystyrene into porous carbon sheets and hollow carbon shells over different magnesium oxide templates for efficient removal of methylene blue. RSC Adv. 5, 105047–105056.

Xue, D., Zhu, D., Liu, M.X., Gan, L.H., 2018. Schiff-base/resin copolymer under hypersaline condition to high-level N-doped porous carbon nanosheets for supercapacitors. ACS Appl. Nano Mater. 1, 4998–5007.

Zhao, Y., Meng, Y., Jiang, P., 2014. Carbon@MnO_2 core-shell nanospheres for flexible high-performance supercapacitor electrode materials. J. Power Sources 259, 219–226.

Zhao, J., Lai, H.W., Lyu, Z.Y., Jiang, Y.F., Wang, X.Z., Jin, Z., Liu, J., Hu, Z., 2015. Hydrophilic hierarchical nitrogen-doped carbon nanocages for ultrahigh supercapacitive performance. Adv. Mater. 27, 3541–3545.

Zhao, J., Jiang, Y.F., Fan, H., Liu, M., Zhuo, Q., Wang, X.Z., Wu, Q., Yang, L.J., Ma, Y.W., Hu, Z., 2017. Porous 3D few-layer graphene-like carbon for ultrahigh-power supercapacitors with well-defined structure-performance relationship. Adv. Mater. 29, 1604569–1604575.